ETH
Eidgenössische Technische Hochschule Zürich
Swiss Federal Institute of Technology Zurich

Seminar for Applied Mathematics SAM

EXPLICIT AND IMPLICIT FINITE VOLUME SCHEMES FOR RADIATION MHD AND THE EFFECTS OF RADIATION ON WAVE PROPAGATION IN STRATIFIED ATMOSPHERES.

S. Mishra and F. Fuchs and A. McMurry and N.H. Risebro

Research Report No. 2013-40
November 2013

Seminar für Angewandte Mathematik
Eidgenössische Technische Hochschule
CH-8092 Zürich
Switzerland

Funding ERC: 306279 SPARCCLE

Manuscript submitted to
AIMS' Journals
Volume **X**, Number **0X**, XX **200X**

doi:10.3934/xx.xx.xx.xx

pp. **X–XX**

EXPLICIT AND IMPLICIT FINITE VOLUME SCHEMES FOR RADIATION MHD AND THE EFFECTS OF RADIATION ON WAVE PROPAGATION IN STRATIFIED ATMOSPHERES.

Franz Fuchs

SINTEF Applied Mathematics
Oslo, Norway

Andrew McMurry, Nils Henrik Risebro

Center of Mathematics for Applications
University of Oslo
Oslo-0316, Norway

Siddhartha Mishra

Seminar for Applied Mathematics (SAM)
ETH Zurich
HG G 57.2, Rämistrasse 101, Zurich-8092, Switzerland

(Communicated by the associate editor name)

Abstract. We present a radiation MHD model based on moments (M1) of the radiative transport equation. This M1 model is approximated numerically by robust finite volume schemes. We compare explicit and semi-implicit schemes and show how radiation affects wave propagation in stratified atmospheres.

1. **The model.** Radiation and plasma dynamics play significant roles in energy transfer by wave propagation in stratified magneto-atmospheres. Such a configuration is modeled [1] by the equations of *stratified radiation magnetohydrodynamics (stratified RMHD)* given by,

$$\begin{aligned}
\rho_t + \operatorname{div}(\rho\mathbf{u}) &= 0,\\
(\rho\mathbf{u})_t + \operatorname{div}\left(\rho\mathbf{u}\otimes\mathbf{u} + \left(p + \frac{1}{2}\left|\bar{\mathbf{B}}\right|^2\right) I - \bar{\mathbf{B}}\otimes\bar{\mathbf{B}}\right) &= -\rho g\mathbf{e}_3,\\
\bar{\mathbf{B}}_t + \operatorname{div}\left(\mathbf{u}\otimes\bar{\mathbf{B}} - \bar{\mathbf{B}}\otimes\mathbf{u}\right) &= 0,\\
E_t + \operatorname{div}\left(\left(E + p + \frac{1}{2}\left|\bar{\mathbf{B}}\right|^2\right)\mathbf{u} - \left(\mathbf{u}\cdot\bar{\mathbf{B}}\right)\bar{\mathbf{B}}\right) &= -\rho g\left(\mathbf{u}\cdot\mathbf{e}_3\right) + \mathcal{Q}^{rad},\\
\operatorname{div}(\bar{\mathbf{B}}) &= 0,
\end{aligned} \tag{1.1a}$$

where ρ is the density, $\mathbf{u} = \{u_1, u_2, u_3\}$ and $\bar{\mathbf{B}} = \{\bar{B}_1, \bar{B}_2, \bar{B}_3\}$ are the velocity and magnetic fields respectively, p is the thermal pressure, g is the constant acceleration

2010 *Mathematics Subject Classification.* Primary: 65M06; Secondary: 35C65.
Key words and phrases. MHD, radiation, explicit and implicit schemes.

due to gravity , $\mathbf{e}_3$ represents the unit vector in the vertical (z-) direction. E is the total energy, for simplicity determined by the ideal gas equation of state:

$$E = \frac{p}{\gamma - 1} + \frac{1}{2}\rho \left|\mathbf{u}\right|^2 + \frac{1}{2}\left|\bar{\mathbf{B}}\right|^2,$$

where $\gamma > 1$ is the adiabatic gas constant.

The term $\mathcal{Q}^{rad}$ in (1.1a) represents energy transfer due to *radiation* and depends on the radiative intensity $I = I(\mathbf{x}, t, \Omega, \nu)$ which is a function of space $\mathbf{x} \in \mathbb{R}^3$, time $t \in \mathbb{R}$, the angle $\Omega \in S^2$ and the frequency $\nu \in \mathbb{R}$. The radiative intensity evolves in accordance with the *time-dependent* radiative transport equation,

$$\frac{1}{c} I_t + \Omega \cdot \nabla_{\mathbf{x}} I = S - \sigma^{\text{ext}} I + \frac{\sigma^{\text{sc}}}{4\pi} \int_{S^2} K(\Omega, \Omega') I(\Omega') d\Omega' d\nu, \tag{1.1b}$$

where $\nabla_{\mathbf{x}}$ denotes the spatial gradient, c is the speed of light, $\sigma^{\text{ext}} = \sigma + \sigma^{\text{sc}}$ is the extinction opacity, σ is the absorption opacity and σ^{sc} is the scattering opacity. Furthermore, $S = S(T)$ is the emission term with $T = \frac{p}{\rho g H}$ being the local temperature. For simplicity, we can assume *locally thermodynamic equilibrium* (LTE) which implies that

$$S = \sigma B(T), \tag{1.2}$$

with $B = aT^4$ being the Planck function. The scattering term in (1.1b) is given in terms of the kernel K. More details regarding the derivation of (1.1) can be checked from [4].

The term $\mathcal{Q}^{rad}$ in (1.1a) is determined by minus the integral over all frequencies ν and angles Ω of the right hand side (sources) of equation (1.1b). Since the integral over the scattering term equals $\sigma^{\text{sc}} I$, this $\mathcal{Q}^{rad}$ is given by the integral of $S - \sigma I$.

The main difficulty associated with the numerical simulation of (1.1) lies in the fact that the radiative intensity is a seven dimensional function as it depends on space (3), time (1), angle (2) and frequency (1) variables. None of the currently available methods are able to resolve such a high-dimensional problem efficiently. Hence, we need to simplify the radiative transport model by reducing dimensions. Notice that the radiative energy flux $\mathcal{Q}^{rad}$ involves integrating over angle and frequency, so a detailed approximation of the radiative intensity may not be necessary in order to account for the role of radiation in MHD.

1.1. **A moments based model (M1) for radiative transfer.**

As we have already pointed out, a direct simulation of the equation for radiative transfer (1.1b) is too costly. An analogous situation prevails in fluid mechanics as the Boltzmann equation modeling mesoscopic scales of the flow is high-dimensional. Suitable macroscopic scale approximations are obtained by taking moments of the Boltzmann equation that yield the Navier-Stokes equations of fluid dynamics, including closure models for completing the system of equations. Similarly, (see [5, 6] and references therein) we consider the first three angular moments of the radiative intensity I in equation (1.1b),

$$\begin{aligned} \mathcal{E} &= \frac{1}{c} \int_{S^2} I(\Omega) d\Omega, \\ \boldsymbol{\mathcal{F}} &= \frac{1}{c} \int_{S^2} \Omega I(\Omega) d\Omega, \\ \mathcal{P} &= \frac{1}{c} \int_{S^2} \Omega \otimes \Omega I(\Omega) d\Omega. \end{aligned} \tag{1.3}$$

Here, $\mathcal{E}(\nu), c\boldsymbol{\mathcal{F}}(\nu)$ and $\mathcal{P}(\nu)$ are the spectral radiative energy, spectral radiative flux and spectral radiative pressure, respectively. All the quantities in the above expressions depend on the frequency variable. For simplicity, we neglect the frequency dependence and therefore work with a uni-group model. A multi-group model with explicit frequency dependence will be considered in a later paper.

Taking the zeroth and first angular moments of (1.1b) and neglecting scattering terms ($\sigma^{\rm sc} = 0$), we obtain the *M1 radiation model* ([5]),

$$\begin{aligned} &\mathcal{E}_t + c\,\mathrm{div}\,\boldsymbol{\mathcal{F}} = c\sigma(aT^4 - \mathcal{E}),\\ &\boldsymbol{\mathcal{F}}_t + c\,\mathrm{div}\,\mathcal{P} = -c\sigma\boldsymbol{\mathcal{F}}. \end{aligned} \tag{1.4}$$

In our units the speed of light is $c = 3 \cdot 10^4$. For wave propagation in stratified atmospheres, the absorption opacity $\sigma(\mathbf{x}, t)$ scales as the density ρ.

The equations have to be closed by specifying the radiative pressure $\mathcal{P}$ in terms of the lower moments. An entropy maximization method was employed in [5] to obtain the following moment closure,

$$\mathcal{P} = D\mathcal{E}, \quad D = \frac{1-\chi}{2}\mathbf{Id} + \frac{3\chi - 1}{2}\frac{\boldsymbol{\mathcal{F}} \otimes \boldsymbol{\mathcal{F}}}{\|\boldsymbol{\mathcal{F}}\|^2}, \quad \chi = \frac{3 + 4f^2}{5 + 2\sqrt{4 - 3f^2}}, \quad f = \left\| \frac{\boldsymbol{\mathcal{F}}}{\mathcal{E}} \right\|. \tag{1.5}$$

Here, $\mathbf{Id}$ is the 3×3 identity matrix, D is referred to as the Eddington tensor and χ as the Eddington factor.

Remark 1.1. *Although, the M1 model is derived by integrating over all angles Ω and frequencies ν, directional information is partly recovered through the radiative flux $c\boldsymbol{\mathcal{F}}$. In addition, frequency dependence can be recovered by using a multi-group model.*

Combining the M1 model (1.4), (1.5) with stratified MHD, based on the Godunov-Powell form and embedded steady states [3], we obtain the following reduced model, henceforth called *reduced stratified radiation MHD equations*,

$$\begin{aligned} &\rho_t + \mathrm{div}(\rho\mathbf{u}) = 0,\\ &(\rho\mathbf{u})_t + \mathrm{div}\left(\rho\mathbf{u}\otimes\mathbf{u} + \left(p + \frac{1}{2}|\mathbf{B}|^2 + \tilde{\mathbf{B}}\cdot\mathbf{B}\right) I - \mathbf{B}\otimes\mathbf{B} - \tilde{\mathbf{B}}\otimes\mathbf{B} - \mathbf{B}\otimes\tilde{\mathbf{B}}\right)\\ &\qquad\qquad = -\left(\mathbf{B} + \tilde{\mathbf{B}}\right)(\mathrm{div}\,\mathbf{B}) - \rho g\mathbf{e}_3,\\ &\mathbf{B}_t + \mathrm{div}\left(\mathbf{u}\otimes\mathbf{B} - \mathbf{B}\otimes\mathbf{u} + \mathbf{u}\otimes\tilde{\mathbf{B}} - \tilde{\mathbf{B}}\otimes\mathbf{u}\right) = -\mathbf{u}(\mathrm{div}\mathbf{B}),\\ &E_t + \mathrm{div}\left(\left(E + p + \frac{1}{2}|\mathbf{B}|^2 + \mathbf{B}\cdot\tilde{\mathbf{B}}\right)\mathbf{u} - (\mathbf{u}\cdot\mathbf{B})\mathbf{B} - \left(\mathbf{u}\cdot\tilde{\mathbf{B}}\right)\tilde{\mathbf{B}}\right)\\ &\qquad\qquad = -(\mathbf{u}\cdot\mathbf{B})(\mathrm{div}\,\mathbf{B}) - \rho g\,(\mathbf{u}\cdot\mathbf{e}_3) - c\sigma(aT^4 - \mathcal{E}),\\ &\mathcal{E}_t + c\,\mathrm{div}\,\boldsymbol{\mathcal{F}} = +c\sigma(aT^4 - \mathcal{E}),\\ &\boldsymbol{\mathcal{F}}_t + c\,\mathrm{div}\,\mathcal{P} = -c\sigma\boldsymbol{\mathcal{F}}. \end{aligned} \tag{1.6}$$

Here, the radiative pressure $\mathcal{P}$ is determined by the moment closure (1.5) and $\tilde{\mathbf{B}}$ is any *potential* background magnetic field with

$$\mathrm{div}(\tilde{\mathbf{B}}) \equiv 0, \quad \mathrm{curl}(\tilde{\mathbf{B}}) \equiv 0.$$

The stratified radiation MHD model (1.6) can be written in the following balance law form,

$$\begin{aligned} \mathbf{U}^{mhd}_t + \operatorname{div}\left(\mathbf{F}^{mhd}(\mathbf{U}^{mhd})\right) &= \mathbf{S}^{GP} + \mathbf{S}^{g} + \mathbf{S}^{rad}(T,\mathcal{E}), \\ \mathbf{U}^{rad}_t + \operatorname{div}\left(\mathbf{F}^{rad}(\mathbf{U}^{rad})\right) &= \tilde{\mathbf{S}}^{rad}(T,\mathcal{E}), \end{aligned} \tag{1.7}$$

where $\mathbf{U}^{mhd} = \{\rho, \mathbf{u}, \mathbf{B}, E\}$ denote the plasma variables and $\mathbf{U}^{rad} = \{\mathcal{E}, \boldsymbol{\mathcal{F}}\}$ are the radiation variables, and $T = \frac{p}{\rho g H}$. Note that (1.7) brings out the split structure of (1.6) quite clearly as the flux $\mathbf{F}^{mhd}$ is independent of $\mathbf{U}^{rad}$, and $\mathbf{F}^{rad}$ is independent of $\mathbf{U}^{mhd}$. The only coupling between the radiative and plasma variables in (1.7) is through the source term $c\sigma(aT^4 - \mathcal{E})$. This split structure can be employed in designing suitable numerical schemes for (1.6) by combining efficient schemes for the ideal MHD equations together with schemes for the M1 model.

It is essential to consider some theoretical properties of (1.6) in order to design robust numerical schemes to approximate the solutions of the stratified RMHD equations.

1.2. **Theoretical properties of the stratified RMHD equations.** The stratified RMHD equations (1.6) have many desirable physical properties. It is important for the design of numerical schemes to inherit those. We summarize some properties below, starting with the hyperbolicity of RMHD.

- **Hyperbolicity.** Consider (1.6) in the x-direction and evaluate the flux Jacobian A of the flux $\mathbf{f} = \left(\mathbf{F}^{mhd}, \mathbf{F}^{rad}\right)$. The split structure of (1.7) is reflected in the block diagonal form of the Jacobian,

  $$A = \begin{pmatrix} A^{mhd} & \mathbf{0} \\ \mathbf{0} & A^{rad} \end{pmatrix},$$

  where A^{mhd}, A^{rad} are the Jacobians corresponding to $\mathbf{F}^{mhd}$ and $\mathbf{F}^{rad}$, respectively. The eigenvalues of A^{mhd} are well-known ([2]), and the eigenvalues of A^{rad} can be explicitly calculated ([6]), and are listed below. The strict hyperbolicity of the M1 model is a consequence of its derivation by an entropy principle.
- **Positivity.** The standard positivity requirement is that

  $$\rho \geq 0, \quad p \geq 0, \quad \mathcal{E} \geq 0. \tag{1.8}$$

  A solution of the stratified RMHD equations (1.6) with initial conditions satisfying (1.8) remains positive for all time, see [6].
- **Flux limitation.** For the eigenvalues to be less than the speed of light, the normalized radiative flux needs to be limited, i.e.

  $$f = \left\| \frac{\boldsymbol{\mathcal{F}}}{\mathcal{E}} \right\| \leq 1. \tag{1.9}$$

  Again, a solution of the stratified RMHD equations (1.6) with initial conditions satisfying (1.9) has a limited flux for all time, see [6].
- **Energy balance.** The variation of the total energy

  $$\tilde{E} = E + \mathcal{E}$$

  is only due to the Godunov-Powell source term and the gravity term in (1.6). In particular, if $\operatorname{div} \mathbf{B} \equiv 0$ and $g = 0$, then the total energy is conserved.

- **Steady states.** The steady state of interest for (1.6) is given by,

$$\begin{aligned} &\mathbf{u} \equiv 0, \quad \mathbf{B} \equiv 0, \quad p = p_0 e^{\frac{-z}{H}}, \quad \rho = \rho_0 e^{\frac{-z}{H}}, \\ &\mathcal{E} = aT_0^4, \quad \boldsymbol{\mathcal{F}} = 0, \end{aligned} \tag{1.10}$$

  where $T_0 = \frac{p_0}{gH\rho_0}$ is the constant model temperature and p_0, $\rho_0 = \frac{p_0}{gHT_0}$ are the pressure and density at the bottom $z = 0$. The embedded magnetic field $\tilde{\mathbf{B}}$ can be ANY divergence- and curl-free field.
- **Asymptotic behavior.** As pointed out in [6], the M1 system recovers the equilibrum diffusion regime for large absorption coefficients σ. That is, as $\sigma \to \infty$ (the limit for an opaque medium), the M1 model recovers the correct equlibrium diffusion equation for the temperature.

Remark 1.2. Eigensystem. *The eigenvalues of the radiation part of the flux in* (1.7)*, i.e.* $\mathbf{F}^{rad}$*, are scaled with the* speed of light c*. Both the* diffusion *and* transport *limit are captured by the equations. At equilibrium, when the flux is zero, i.e.* $f = \|\mathbf{f}\| = 0$*, the correct* diffusion limit *is recovered. That is,* $\mathcal{P} = \mathcal{E}/3$ *and the largest eigenvalues are* $\lambda^{\pm} = \pm\frac{c}{\sqrt{3}}$*.On the other hand, in the case of extreme non-equilibrium, i.e.* $\|\mathbf{f}\| = 1$*, the proper* transport limit *is recovered, i.e.* $\mathcal{P} = \mathcal{E}$*. Regarding the eigenvalues in this case, we have that the largest eigenvalues are* $\lambda_{\pm} = \pm c$*.*

In 2 dimensions the eigenvalues of the Jacobian A^{rad} can be explicitly calculated to be (see [6])

$$\begin{aligned} \lambda^{\pm} &= c\left(\frac{f_1}{\xi} \pm \frac{\sqrt{2(\xi-1)(\xi+2)(2(\xi-1)(\xi+2)+3f_3^2)}}{\sqrt{3}\xi(\xi+2)}\right), \\ \lambda^0 &= \frac{c(2-\xi)f_1}{f^2}. \end{aligned} \tag{1.11}$$

Here, $\xi = \sqrt{4-3f^2}$ and $f = (f_1, f_3) = (\frac{\boldsymbol{\mathcal{F}}^1}{\mathcal{E}}, \frac{\boldsymbol{\mathcal{F}}^3}{\mathcal{E}})$. The eigenvalues of the Jacobian in the z-direction can be calculated by replacing f_1 with f_3 in the above expression. The eigenvalues of the Jacobian in 2d are depicted in figure 1. It is easy to see that

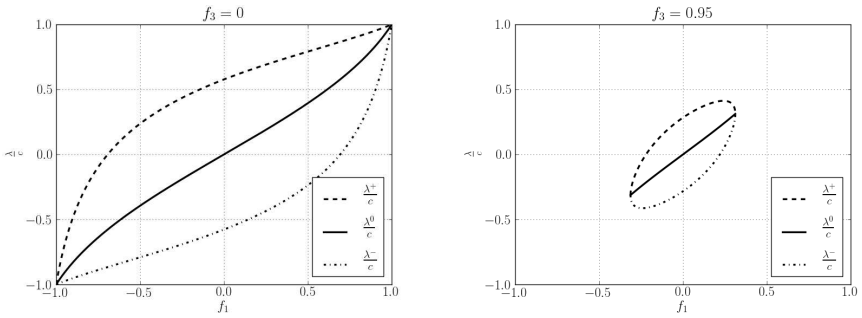

FIGURE 1. The dimensionless eigenvalues of M1 in 2d.

the eigenvalues coincide if $\|f\| = 1$, i.e. we have that

$$\lambda^+ = \lambda^0 = \lambda^- = cf_1, \quad \text{if } \|f\| = 1.$$

Moreover, the characteristic fields associated with $\lambda^{\pm}$ are genuinely nonlinear, whereas the field associated with λ^0 is linearly degenerate, see [6].

Remark 1.3. Diffusion limit and boundary conditions. *The diffusion limit ($f = 0$) is of importance for simulations concerning the solar atmosphere, as the bottom boundary conditions can be derived by using this limit. At the bottom of the photosphere the Sun becomes opaque to visible light, i.e. $\sigma \to \infty$. The asymptotic behavior as $\sigma \to \infty$ is captured by the diffusion limit where $f = 0$. Therefore, the bottom boundary condition for the radiative flux should be*

$$\boldsymbol{\mathcal{F}}(z = 0) = \mathbf{0}, \tag{1.12}$$

and for the radiative energy we can use Neumann boundary conditions or set $\mathcal{E}(z = 0) = aE^4(z = 0)$.

Due to the steady state structure we can model waves in stratified atmospheres (at least in the chromosphere) as perturbations of an equilibrium given in equation (1.10). Waves introduced at the bottom boundary will perturb the radiative equilibrium as they move up the domain and numerical simulations will be focused on the dynamical behavior. However, the main difficulty in numerical computations is, that the fastest wave speeds for equation (1.6) are of the order of the speed of light. Hence, they are much faster than the fast magneto-sonic waves in stratified MHD. According to the CFL condition, an explicit numerical scheme will suffer from a severe restriction of the time step of the order of $\Delta t = \mathcal{O}(\Delta x/c)$. In the following, we will describe a semi-implicit scheme that circumvents this problem and compare it to the explicit scheme.

2. **Finite volume schemes.** We need to design a robust and efficient finite volume scheme that preserves at least some of the properties outlined above. For simplicity, we approximate (1.6) in a Cartesian domain $\mathbf{x} = (x, y, z) \in [X_l, X_r] \times [Y_l, Y_r] \times [Z_b, Z_t]$ and discretize it by a uniform grid in all directions with the grid spacing $\Delta x, \Delta y$ and Δz. We set $x_i = X_l + i\Delta x$, $y_j = Y_l + j\Delta y$ and $z_k = Z_b + k\Delta z$. The indices are $0 \le i \le N_x$, $0 \le j \le N_y$ and $0 \le k \le N_z$. Set $x_{i+1/2} = x_i + \Delta x/2$, $y_{j+1/2} = y_j + \Delta y/2$ and $z_{k+1/2} = z_k + \Delta z/2$, and let $\mathcal{C}_{i,j,k} = [x_{i-1/2}, x_{i+1/2}) \times [y_{j-1/2}, y_{j+1/2}) \times [z_{k-1/2}, z_{k+1/2})$ denote a typical cell. The cell average of the unknown state vector $\mathbf{U}$ over $\mathcal{C}_{i,j,k}$ at time t^n is denoted $\mathbf{U}_{i,j,k}$. Given the decoupled structure of the RMHD equations (1.7), we use the following finite volume scheme (in semi-discrete form),

$$\begin{aligned}
\frac{d}{dt}\mathbf{U}^{mhd}_{i,j,k} &= -\frac{1}{\Delta x}(\tilde{\mathbf{F}}^{1,mhd}_{i+1/2,j,k} - \tilde{\mathbf{F}}^{1,mhd}_{i-1/2,j,k}) - \frac{1}{\Delta y}(\tilde{\mathbf{F}}^{2,mhd}_{i,j+1/2,k} - \tilde{\mathbf{F}}^{2,mhd}_{i,j-1/2,k}) \\
&\quad - \frac{1}{\Delta z}(\tilde{\mathbf{F}}^{3,mhd}_{i,j,k+1/2} - \tilde{\mathbf{F}}^{3,mhd}_{i,j,k-1/2}) + \tilde{\mathbf{S}}^{1}_{i,j,k} + \tilde{\mathbf{S}}^{2}_{i,j,k} + \tilde{\mathbf{S}}^{3}_{i,j,k} + \mathbf{S}^{g}_{i,j,k} + \mathbf{S}^{rad}_{i,j,k}, \\
\frac{d}{dt}\mathbf{U}^{rad}_{i,j,k} &= -\frac{1}{\Delta x}(\tilde{\mathbf{F}}^{1,rad}_{i+1/2,j,k} - \tilde{\mathbf{F}}^{1,rad}_{i-1/2,j,k}) - \frac{1}{\Delta y}(\tilde{\mathbf{F}}^{2,rad}_{i,j+1/2,k} - \tilde{\mathbf{F}}^{2,rad}_{i,j-1/2,k}) \\
&\quad - \frac{1}{\Delta z}(\tilde{\mathbf{F}}^{3,rad}_{i,j,k+1/2} - \tilde{\mathbf{F}}^{3,rad}_{i,j,k-1/2}) + \tilde{\mathbf{S}}^{rad}_{i,j,k}.
\end{aligned} \tag{2.1}$$

Here

$$\mathbf{U}^{mhd}_{i,j,k} = \{\rho_{i,j,k}, \mathbf{u}_{i,j,k}, \mathbf{B}_{i,j,k}, E_{i,j,k}\}, \quad \mathbf{U}^{rad}_{i,j,k} = \{\mathcal{E}_{i,j,k}, \boldsymbol{\mathcal{F}}_{i,j,k}\},$$

are cell averages of the unknowns in the cell $\mathcal{C}_{i,j,k}$. The numerical fluxes $\tilde{\mathbf{F}}^{1,mhd}_{i+1/2,j,k}$, $\tilde{\mathbf{F}}^{2,mhd}_{i,j+1/2,k}$ and $\tilde{\mathbf{F}}^{3,mhd}_{i,j,k+1/2}$, the Godunov Powell sources $\tilde{\mathbf{S}}^{1,2,3}_{i,j,k}$, and the gravity source $\mathbf{S}^{g}_{i,j,k}$ are

all independent of $\mathbf{U}^{rad}_{i,j,k}$. We can therefore directly use any numerical scheme devised for approximating the solutions of stratified MHD equations. In particular, the *well-balanced* three-wave HLLC fluxes with the *upwind* discretization of the Godunov-Powell source terms $\mathbf{S}^{1,2,3}$ of (1.7) described in [3] is a suitable choice. In this case, the gravity term $\mathbf{S}^{g}$ is discretized in a well balanced manner (see [3]) that differs from the standard pointwise evaluation of the source. We are left with having to design suitable discretizations of $\tilde{\mathbf{F}}^{rad}$ and the source terms $S^{rad}, \tilde{S}^{rad}$. We start by describing an explicit discretization. Due to the large restriction on the time step for an explicit scheme in this case, we propose a semi-implicit scheme that allows for much larger time steps.

2.1. **Explicit discretization of the radiative terms.** The key step in completing (2.1) is to define the radiation flux $\tilde{\mathbf{F}}^{rad}$. For simplicity, we choose an HLL two-wave flux. We start with the description of the numerical flux $\tilde{\mathbf{F}}^{1,rad}_{i+1/2.j,k}$ which is defined in terms of an approximate solution to the following Riemann problem,

$$\begin{aligned}
\mathcal{E}_t + c\boldsymbol{\mathcal{F}}^1_x &= 0,\\
\boldsymbol{\mathcal{F}}^1_t + c(\mathcal{E}D^1)_x &= 0,\\
\boldsymbol{\mathcal{F}}^2_t + c(\mathcal{E}D^2)_x &= 0,\\
\boldsymbol{\mathcal{F}}^3_t + c(\mathcal{E}D^3)_x &= 0,\\
\mathbf{U}^{rad}(x,t^n) &= \begin{cases} \mathbf{U}^{rad}_L = \mathbf{U}^{rad}_{i,j,k}, & \text{if} \quad x \le x_{i+1/2},\\ \mathbf{U}^{rad}_R = \mathbf{U}^{rad}_{i+1,j,k}, & \text{if} \quad x > x_{i+1/2}, \end{cases}
\end{aligned} \tag{2.2}$$

Here,

$$D^1 = \frac{1-\chi}{2} + \frac{3\chi-1}{2}\frac{(\boldsymbol{\mathcal{F}}^1)^2}{\|\boldsymbol{\mathcal{F}}\|^2}, \quad D^2 = \frac{3\chi-1}{2}\frac{\boldsymbol{\mathcal{F}}^1\boldsymbol{\mathcal{F}}^2}{\|\boldsymbol{\mathcal{F}}\|^2}, \quad D^3 = \frac{3\chi-1}{2}\frac{\boldsymbol{\mathcal{F}}^1\boldsymbol{\mathcal{F}}^3}{\|\boldsymbol{\mathcal{F}}\|^2}, \tag{2.3}$$

and χ is the Eddington factor defined in (1.5).

We approximate the solution of (2.2) with the following wave structure,

$$\mathbf{U}^{rad}_{H2} = \begin{cases} \mathbf{U}^{rad}_L & \text{if } \frac{x}{t} \le s_L,\\ \mathbf{U}^{rad}_* & \text{if } s_L < \frac{x}{t} < s_R,\\ \mathbf{U}^{rad}_R & \text{if } s_R \le \frac{x}{t}, \end{cases} \qquad \mathbf{F}^{1,rad}_{H2} = \begin{cases} \mathbf{F}^{1,rad}_L & \text{if } \frac{x}{t} \le s_L,\\ \mathbf{F}^{1,rad}_* & \text{if } s_L < \frac{x}{t} < s_R,\\ \mathbf{F}^{1,rad}_R & \text{if } s_R \le \frac{x}{t}. \end{cases} \tag{2.4}$$

Note that we have used the standard HLL two-wave solver in (2.4). A straightforward calculation using the Rankine-Hugoniot condition leads to the following middle flux,

$$\mathbf{F}^{1,rad}_* = \frac{s_R\mathbf{F}^{1,rad}_L - s_L\mathbf{F}^{1,rad}_R + s_Ls_R(\mathbf{U}^{rad}_R - \mathbf{U}^{rad}_L)}{s_R - s_L}. \tag{2.5}$$

The resulting numerical flux is

$$\tilde{\mathbf{F}}^{1,rad}_{i+1/2,j,k} = \begin{cases} \mathbf{F}^{1,rad}_{i,j,k} & , \text{ if } (s_L)_{i+1/2,j,k} > 0,\\ \mathbf{F}^{1,rad,*}_{i,j,k} & , \text{ if } (s_L)_{i+1/2,j,k} \le 0 \wedge (s_R)_{i+1/2,j,k} \ge 0,\\ \mathbf{F}^{1,rad}_{i+1,j,k} & , \text{ if } (s_R)_{i+1/2,j,k} < 0. \end{cases} \tag{2.6}$$

Choice of wave speeds. The wave speeds $s_{L,R}$ in (2.4) need to be chosen suitably. As they approximate the fastest waves in the M1-system (1.4), the simplest stable choice of wave speeds is,

$$s_L = -c, \quad s_R = +c, \tag{2.7}$$

where c is the constant speed of light. Note that this choice leads to a Rusanov type scheme (with a global $s_L = -s_R$ rather than a local one) for the M1 model. That means we always use the middle state and the numerical flux is given by

$$\tilde{\mathbf{F}}^{1,rad}_{i+1/2,j,k} = \frac{1}{2}(\mathbf{F}^{1,rad}_{i,j,k} + \mathbf{F}^{1,rad}_{i+1,j,k}) - \frac{c}{2}(\mathbf{U}^{rad}_{i+1,j,k} - \mathbf{U}^{rad}_{i,j,k}). \tag{2.8}$$

This choice will be dissipative (particularly at first order) but some accuracy is recovered with a second-order approximation.

A more accurate choice follows [6] and leads to,

$$\begin{aligned} s_L &= \min\{0, cf^1_L, c\frac{f^1_L - \chi_L}{1 - f^1_l}, c\frac{f^1_L - \chi_L}{1 + f^1_l}, \lambda^-(\mathbf{U}^{rad}_L)\}, \\ s_R &= \max\{0, cf^1_R, c\frac{f^1_R - \chi_R}{1 - f^1_l}, c\frac{f^1_R - \chi_R}{1 + f^1_l}, \lambda^+(\mathbf{U}^{rad}_R)\}, \end{aligned} \tag{2.9}$$

where $f^1 = \frac{\boldsymbol{\mathcal{F}}^1}{\mathcal{E}}$, and $\chi^{L,R} = \chi(f^1_{L,R})$ is the Eddington factor (1.5). Similarly, $\lambda^\pm$ are the eigenvalues for a given state defined in (1.11). The results of [6] show that the above choice is robust.

The fluxes in the y- and z-directions are obtained by replacing the appropriate quantities in (2.5) and (2.6). This completes the description of the scheme (2.1). Second-order accuracy can be obtained by the reconstruction routines of [3].

Radiative source terms. We are left with describing the discretization of the radiative source terms. The simplest way would be a point-wise evolution of the source at the current time step n (explicit). But, depending on the constants the source term is potentially stiff. Hence, we use an implicit discretization of the radiative source term.

$$\begin{aligned} \mathbf{S}^{rad,n+1}_{i,j,k} &= \{0, \mathbf{0}, \mathbf{0}, -c\sigma^{n+1}_{i,j,k}(a(T^{n+1}_{i,j,k})^4 - \mathcal{E}^{n+1}_{i,j,k})\}, \\ \tilde{\mathbf{S}}^{rad,n+1}_{i,j,k} &= \{c\sigma^{n+1}_{i,j,k}(a(T^{n+1}_{i,j,k})^4 - \mathcal{E}^{n+1}_{i,j,k}), c\sigma^{n+1}_{i,j,k}\boldsymbol{\mathcal{F}}^{n+1}_{i,j,k}\}. \end{aligned} \tag{2.10}$$

Observe, that we still call our scheme explicit, although we discretize the radiation sources implicitly. This is because it is only locally implicit and the resulting nonlinear systems can be solved for each cell independently.

The main difficulty associated with (2.1) is the presence of time scales dominated by the speed of light c, dictating a very small time step for explicit finite volume schemes. However, we are only interested in the effect of radiation on the plasma (stratified MHD equation) and do not need to approximate the solutions of the M1 model accurately. Therefore, we devise semi-implicit schemes in the next section that remove this limitation on the time step.

2.2. **Semi-implicit solvers for Radiation-MHD.** In typical applications, the fast magneto-acoustic wave speeds are at least two to three orders of magnitude smaller than the speed of light c. Hence, due to the CFL condition any explicit scheme desigend to resolve time scales of the MHD model will be extremely slow. In order to be able to do realistic simulations, we need to devise semi-implicit schemes that allow us to increase the time step by some orders of magnitude. In this section we will describe semi-implicit solvers for approximating the solutions of RMHD (1.6). Since the only coupling of the MHD part to the M1 model for radiative transport is given by the source term, we can devide our numerical scheme into two parts.

We discretize the MHD part, i.e. the fluxes $\mathbf{F}^{mhd}$, the Powell source $\mathbf{S}^{GP}$ and the gravity source $\mathbf{S}^g$ explicitly. The M1 model along with the radiative source $\mathbf{S}^{rad}$

in the energy equation on the other hand are discretized in an implicit manner. We present the resulting nonlinear system that has to be solved in order to get an approximation to the solution at the next time level. For the sake of clarity we restrict ourself to one space dimension in the description. It is straightforward to extend this approach to several space dimensions. In one dimension we set $(\mathcal{F}^2, \mathcal{F}^3) = (0, 0)$ and the system of equations to be discretized implicitly simplifies to

$$\begin{aligned} E_t + H &= -c\sigma(aT^4 - \mathcal{E}), \\ \mathcal{E}_t + c\mathcal{F}^1_x &= +c\sigma(aT^4 - \mathcal{E}), \\ \mathcal{F}^1_t + c(\mathcal{E}\chi)_x &= -c\sigma\mathcal{F}^1. \end{aligned} \tag{2.11}$$

Here, H contains the energy-flux, the gravity source and the Powell source of the energy equation. The semi-implicit numerical solver has the following form

$$\begin{aligned} E_i^{n+1} - E_i^n + \Delta t H^n &= -\Delta t c\sigma_i^{n+1}(a(T_i^{n+1})^4 - \mathcal{E}_i^{n+1}), \\ \mathcal{E}_i^{n+1} - \mathcal{E}_i^n + \frac{\Delta t}{\Delta x}(A_{i+1/2}^{n+1} - A_{i-1/2}^{n+1}) &= +\Delta t c\sigma_i^{n+1}(a(T_i^{n+1})^4 - \mathcal{E}_i^{n+1}), \\ \mathcal{F}_i^{1,n+1} - \mathcal{F}_i^{1,n} + \frac{\Delta t}{\Delta x}(B_{i+1/2}^{n+1} - B_{i-1/2}^{n+1}) &= -\Delta t c\sigma_i^{n+1}\mathcal{F}_i^{1,n+1}. \end{aligned} \tag{2.12}$$

Note that the discretization of H in the energy equation is explicit and is readily provided by the solver for the MHD part of equation (1.6). Using the first order HLL flux (2.8) with $s_R = -s_L = c$, the flux differences simplify to

$$\begin{aligned} A_{i+1/2}^{n+1} - A_{i-1/2}^{n+1} &= \frac{c}{2}(\mathcal{F}_{i+1}^{1,n+1} - \mathcal{F}_{i-1}^{1,n+1} - \mathcal{E}_{i+1}^{n+1} + 2\mathcal{E}_i^{n+1} - \mathcal{E}_{i-1}^{n+1}), \\ B_{i+1/2}^{n+1} - B_{i-1/2}^{n+1} &= \frac{c}{2}(\mathcal{E}_{i+1}^{n+1}\chi_{i+1}^{n+1} - \mathcal{E}_{i-1}^{n+1}\chi_{i-1}^{n+1} - \mathcal{F}_{i+1}^{1,n+1} + 2\mathcal{F}_i^{1,n+1} - \mathcal{F}_{i-1}^{1,n+1}). \end{aligned} \tag{2.13}$$

The update at the new time level $\xi_i = (\vec{\alpha}, \vec{\beta}, \vec{\delta})_i = (E_i^{n+1}, \mathcal{E}_i^{n+1}, \mathcal{F}_i^{n+1})$ is given by finding a root of the following function

$$F_i(\vec{\alpha}, \vec{\beta}, \vec{\delta}) = \begin{pmatrix} \alpha_i - E_i^n + \Delta t H^n + \Delta t c\sigma_i^{n+1}(w_i^{n+1}(\alpha_i - v_i^{n+1})^4 - \beta_i) \\ \beta_i - \mathcal{E}_i^n + \frac{\Delta t}{\Delta x}A(\xi_{i-1}, \xi_i, \xi_{i+1}) - \Delta t c\sigma_i^{n+1}(w_i^{n+1}(\alpha_i - v_i^{n+1})^4 - \beta_i) \\ \delta_i - \mathcal{F}_i^n + \frac{\Delta t}{\Delta x}B(\xi_{i-1}, \xi_i, \xi_{i+1}) + \Delta t c\sigma_i^{n+1}\delta_i \end{pmatrix}, \tag{2.14}$$

where we have defined $w_i^{n+1} = a\left(\frac{\gamma-1}{\rho_i^{n+1}}\right)^4$ and $v_i^{n+1} = \frac{1}{2}\rho_i^{n+1}(\mathbf{u}_i^{n+1})^2 + \frac{1}{2}(\bar{\mathbf{B}}_i^{n+1})^2$. The values of ρ_i^{n+1}, $\mathbf{u}_i^{n+1}$, $\bar{\mathbf{B}}_i^{n+1}$ and H^n are directly available from the explicit solver for the MHD equations. The expressions for the fluxes A and B depend on the flux discretization. For the flux (2.8) we have that

$$\begin{aligned} A(\xi_{i-1}, \xi_i, \xi_{i+1}) &= \frac{c}{2}(\delta_{i+1} - \delta_{i-1} - \beta_{i+1} + 2\beta_i - \beta_{i-1}), \\ B(\xi_{i-1}, \xi_i, \xi_{i+1}) &= \frac{c}{2}\left(\beta_{i+1}\chi\left(\frac{|\delta_{i+1}|}{\beta_{i+1}}\right) - \beta_{i-1}\chi\left(\frac{|\delta_{i-1}|}{\beta_{i-1}}\right) - \delta_{i+1} + 2\delta_i - \delta_{i-1}\right). \end{aligned} \tag{2.15}$$

A solution ξ' with $F(\xi') = 0$ provides the values at the new time level $n+1$, namely $(E_i^{n+1}, \mathcal{E}_i^{n+1}, \mathcal{F}_i^{n+1}) = \xi_i'$. In order to find a root of $F(\xi)$ we use Newton iteration

$$DF(\xi_j)(\xi_{j+1} - \xi_j) = -F(\xi_j), \tag{2.16}$$

with the start value $(\xi_0)_i = (E_i^n, \mathcal{E}_i^n, \mathcal{F}_i^n)$. We stop the iteration, if $\|F(\xi_j)\| \leq \text{tol}$ or after a certain number of iterations. The Jacobian has the following structure

$$DF = \begin{pmatrix} DF_{1,1} & DF_{1,2} & 0 \\ DF_{2,1} & DF_{2,2} & DF_{2,3} \\ 0 & DF_{3,2} & DF_{3,3} \end{pmatrix}, \tag{2.17}$$

where $DF_{1,1}$, $DF_{1,2}$ and $DF_{2,1}$ are diagonal matrices with the diagonal entries given by $df_{1,1} = 1 + 4\Delta t c\sigma_i^{n+1} w_i^{n+1}(x_i^1 - v_i^{n+1})^3$, $df_{1,2} = -\Delta t c\sigma_i^{n+1}$ and $df_{2,1} = -\Delta t c\sigma_i^{n+1} w_i^{n+1}(x_i^1 - v_i^{n+1})^3$, respectively.

For $p, q \in \{2, 3\}$ we have the following tridiagonal structure

$$DF_{p,q} = \begin{pmatrix} \ddots & \ddots & 0 & 0 & 0 \\ \ddots & \ddots & \ddots & 0 & 0 \\ 0 & dl_{p,q} & d_{p,q} & dr_{p,q} & 0 \\ 0 & 0 & \ddots & \ddots & \ddots \\ 0 & 0 & 0 & \ddots & \ddots \end{pmatrix}. \tag{2.18}$$

The components of $DF_{2,2}$ and $DF_{2,3}$ can be calculated as

$$\begin{aligned} dl_{2,2} = dr_{2,2} = -\frac{c\Delta t}{2\Delta x}, d_{2,2} = 1 + \Delta t c\sigma_i^{n+1} + \frac{c\Delta t}{\Delta x}, \\ dl_{2,3} = -\frac{c\Delta t}{2\Delta x}, dr_{2,3} = +\frac{c\Delta t}{2\Delta x}, d_{2,3} = 0. \end{aligned} \tag{2.19}$$

The derivatives of the third component of F are more complicated, due to the non-linearity of the flux function. However, for the Newton iteration to work we only need an approximation of the Jacobian of F. The function χ is a monotone function with $\frac{1}{3} \leq \chi \leq 1$. It is therefore reasonable to assume that χ is independent of $\frac{\boldsymbol{\mathcal{F}}}{\mathcal{E}}$ in order to approximate the Jacobian. That means we have

$$\frac{\partial \beta_i \chi\left(\frac{|\delta_i|}{\beta_i}\right)}{\partial \beta_i} \approx \chi\left(\frac{|\delta_i|}{\beta_i}\right), \quad \frac{\partial \beta_i \chi\left(\frac{|\delta_i|}{\beta_i}\right)}{\partial \delta_i} \approx 0. \tag{2.20}$$

Using this assumpition, it follows that the compontents of $DF_{3,2}$ and $DF_{3,3}$ are given by

$$\begin{aligned} dl_{3,2} = -\frac{c\Delta t}{2\Delta x}\chi_{i-1}, dr_{3,2} = +\frac{c\Delta t}{2\Delta x}\chi_{i+1}, d_{3,2} = 0, \\ dl_{3,3} = dr_{3,3} = -\frac{c\Delta t}{2\Delta x}, d_{3,3} = 1 + \Delta t c\sigma_i^{n+1} + \frac{c\Delta t}{\Delta x}. \end{aligned} \tag{2.21}$$

This concludes the description of the implicit solver for the interior points. For the Newton (2.16) iteration to be complete, we need to implement boundary conditions for both the right hand side F and the Jacobian DF. Using Neumann boundary conditions for the M_1 model in the explicit solver, translates to the following boundary conditions for the implicit solver. For $F(x)$ in equation (2.14) we

need to define values for the spatial derivatives at the boundaries, namely

$$\begin{aligned}
A(\xi_0,\xi_1,\xi_2) &= \frac{c}{2}(\delta_2-\delta_1-\beta_2+\beta_1),\\
A(\xi_{N_x-1},\xi_{N_x},\xi_{N_x+1}) &= \frac{c}{2}(\delta_{N_x}-\delta_{N_x-1}+\beta_{N_x}-\beta_{N_x-1}),\\
B(\xi_0,\xi_1,\xi_2) &= \frac{c}{2}\left(\beta_2\chi\left(\frac{|\delta_2|}{\beta_2}\right)-\beta_1\chi\left(\frac{|\delta_1|}{\beta_1}\right)-\delta_2+\delta_1\right),\\
B(\xi_{N_x-1},\xi_{N_x},\xi_{N_x+1}) &= \frac{c}{2}\left(\beta_{N_x}\chi\left(\frac{|\delta_{N_x}|}{\beta_{N_x}}\right)-\beta_{N_x-1}\chi\left(\frac{|\delta_{N_x-1}|}{\beta_{N_x-1}}\right)+\delta_{N_x}-\delta_{N_x-1}\right).
\end{aligned} \tag{2.22}$$

Furthermore, for the Jacobian DF in (2.17) we define

$$\chi\left(\frac{|\delta_{N_x+1}|}{\beta_{N_x+1}}\right)=\chi\left(\frac{|\delta_{N_x}|}{\beta_{N_x}}\right),\quad \chi\left(\frac{|\delta_0|}{\beta_0}\right)=\chi\left(\frac{|\delta_1|}{\beta_1}\right) \tag{2.23}$$

at the boundaries. For different types of boundary conditions those definitions will change.

This semi-implicit approach is easily extended to multi space dimensions. We omit the description in this article, and continue with describing the properties of the various schemes.

2.3. **Properties of the explicit and semi-implicit schemes.** We consider finite volume schemes of type (2.1) approximating the solutions of the stratified RMHD equations (1.6). In the numerical experiments of this paper we choose to test and compare the following two numerical schemes. Since it is essential to preserve discrete versions of the steady states, we use the *well-balanced* three-wave HLLC solver of [3] (with the corresponding discretiziations of the Powell source and the gravitational source term as well as the balanced Neumann type boundary conditions). For the radiative part of (1.6) we choose the HLL solver described in sections 2.1 and 2.2.

Therefore, we have the following two possiblities.

- Explicit solver $M_{\mathrm{HLLC}}R_{\mathrm{HLL}_e}$: explicit well-balanced HLLC solver for MHD combined with the explicit HLL scheme for the radiation part, and
- semi-implicit solver $M_{\mathrm{HLLC}}R_{\mathrm{HLL}_i}$: explicit well-balanced HLLC solver for MHD combined with the implicit HLL scheme for the radiation part.

We want to remark that the fully explicit solver $M_{\mathrm{HLLC}}R_{\mathrm{HLL}_e}$ uses a locally implicit time discretization for the sources radiative sources. In one dimension the general numerical scheme has the form

$$\begin{aligned}
\mathbf{U}^{mhd,n+1}_{i,j,k}-\mathbf{U}^{mhd,n}_{i,j,k}+\frac{\Delta t}{\Delta x}(\tilde{\mathbf{F}}^{1,mhd,n}_{i+1/2,j,k}-\tilde{\mathbf{F}}^{1,mhd,n}_{i-1/2,j,k}) &= \Delta t\tilde{\mathbf{S}}^{1,n}_{i,j,k}+\Delta t\mathbf{S}^{g,n}_{i,j,k}+\Delta t\mathbf{S}^{rad,n+1}_{i,j,k},\\
\mathcal{E}^{n+1}_{i,j,k}(1+\Delta tc\sigma^{n+1}_{i,j,k})-\mathcal{E}^{n}_{i,j,k}+\frac{\Delta t}{\Delta x}(A^{p}_{i+1/2,j,k}-A^{p}_{i-1/2,j,k}) &= +\Delta tc\sigma^{n+1}_{i,j,k}a(T^{n+1}_{i,j,k})^4,\\
\mathcal{F}^{1,n+1}_{i,j,k}(1+\Delta tc\sigma^{n+1}_{i,j,k})-\mathcal{F}^{1,n}_{i,j,k}+\frac{\Delta t}{\Delta x}(B^{1,p}_{i+1/2,j,k}-B^{1,p}_{i-1/2,j,k}) &= 0,\\
\mathcal{F}^{2,n+1}_{i,j,k}(1+\Delta tc\sigma^{n+1}_{i,j,k})-\mathcal{F}^{2,n}_{i,j,k}+\frac{\Delta t}{\Delta x}(B^{2,p}_{i+1/2,j,k}-B^{2,p}_{i-1/2,j,k}) &= 0,\\
\mathcal{F}^{3,n+1}_{i,j,k}(1+\Delta tc\sigma^{n+1}_{i,j,k})-\mathcal{F}^{3,n}_{i,j,k}+\frac{\Delta t}{\Delta x}(B^{3,p}_{i+1/2,j,k}-B^{3,p}_{i-1/2,j,k}) &= 0,
\end{aligned} \tag{2.24}$$

where we get the explicit scheme $M_{\mathrm{HLLC}}R_{\mathrm{HLL}_e}$ for $p = n$, and the semi-implicit scheme $M_{\mathrm{HLLC}}R_{\mathrm{HLL}_i}$ for $p = n+1$. Moreover, the flux differences for the Rusanov type scheme are given by

$$\begin{aligned} A^p_{i+1/2} - A^p_{i-1/2} &= \frac{c}{2}(\mathcal{F}^{1,p}_{i+1} - \mathcal{F}^{1,p}_{i-1} - \mathcal{E}^p_{i+1} + 2\mathcal{E}^p_i - \mathcal{E}^p_{i-1}), \\ B^{k,p}_{i+1/2} - B^{k,p}_{i-1/2} &= \frac{c}{2}(\mathcal{E}^p_{i+1}D^{k,p}_{i+1} - \mathcal{E}^p_{i-1}D^{k,p}_{i-1} - \mathcal{F}^{k,p}_{i+1} + 2\mathcal{F}^{k,p}_i - \mathcal{F}^{k,p}_{i-1}), \end{aligned} \tag{2.25}$$

with D^k defined in (2.3).

In the following theorem we summarize the properties of the finite volume schemes $M_{\mathrm{HLLC}}R_{\mathrm{HLL}_e}$, $M_{\mathrm{HLLC}}R_{\mathrm{HLL}_i}$ approximating the solutions of the stratified RMHD equations (1.6).

Theorem 2.1. *Consider the finite volume schemes $M_{HLLC}R_{HLL_e}$, $M_{HLLC}R_{HLL_i}$ approximating the solutions of equation (1.6). Both schemes*

- *are consistent with (1.6) and first order accurate in both space and time (for smooth solutions),*
- *preserve $\mathcal{E} \geq 0$ and $\|\boldsymbol{\mathcal{F}}/\mathcal{E}\| \leq 1$ discretely provided $c, a, \sigma \geq 0$,*
- *are well-balanced, i.e. preserve discrete versions of the steady states (1.10) for any background magnetic field $\tilde{\mathbf{B}}$.*

Proof. The schemes are first order accurate by construction

Next, we show positivity and flux limitation for the explicit scheme. In 1d we have $\mathcal{F}^{2,n}_i = \mathcal{F}^{3,n}_i = 0$. Let us assume that for a fixed n, the two inequalities

$$\mathcal{E}^n_i \geq 0, |\mathcal{F}^{1,n}_i| \leq \mathcal{E}^n_i \tag{2.26}$$

hold true for all i. In that case we can write $\pm\mathcal{F}^{1,n}_i - \mathcal{E}^n_i \leq 0$, which will be used several times in the sequel. Then from the discrete equation (2.24) for radiative energy

$$\mathcal{E}^{n+1}_i(1+\Delta tc\sigma^{n+1}) = \mathcal{E}^n_i - \frac{c\Delta t}{2\Delta x}(\mathcal{F}^{1,n}_{i+1} - \mathcal{F}^{1,n}_{i-1} - \mathcal{E}^n_{i+1} + 2\mathcal{E}^n_i - \mathcal{E}^n_{i-1}) + \Delta tc\sigma^{n+1}a(T^{n+1}_i)^4,$$

we can conclude that

$$\mathcal{E}^{n+1}_i(1+\Delta tc\sigma^{n+1}) \geq \mathcal{E}^n_i - \frac{\Delta t}{\Delta x}c\mathcal{E}^n_i + \Delta tc\sigma^{n+1}a(T^{n+1}_i)^4 \geq \mathcal{E}^n_i(1 - \frac{\Delta t}{\Delta x}c),$$

by using that $\pm\mathcal{F}^{1,n}_i - \mathcal{E}^n_i \leq 0$. So we have that the radiative energy remains positive, if the CFL condition $\Delta t \leq \frac{\Delta x}{c}$ is fulfilled.

In order to show that the flux is limited, we proceed as follows. Assume that (2.26) holds true for a fixed n and all i. Then we need the prove the following two inequalities $\pm\mathcal{F}^{1,n+1}_i - \mathcal{E}^{n+1}_i \leq 0$, using that we have already shown that $\mathcal{E}^n_i \geq 0$ for all i and n. For the scheme (2.24), we have

$$\begin{aligned} (\pm\mathcal{F}^{1,n+1}_i - \mathcal{E}^{n+1}_i)(1+\Delta tc\sigma^{n+1}) =& (\pm\mathcal{F}^{1,n}_i - \mathcal{E}^n_i)(1 - \frac{\Delta t}{\Delta x}c) + \Delta tc\sigma^{n+1}_i a(T^{n+1}_i)^4 \\ &- \frac{c\Delta t}{2\Delta x}(\pm\mathcal{E}^n_{i+1}\chi^n_{i+1} \mp \mathcal{E}^n_{i-1}\chi^n_{i-1} \mp \mathcal{F}^{1,n}_{i+1} \mp \mathcal{F}^{1,n}_{i-1} - \mathcal{F}^{1,n}_{i+1} + \mathcal{F}^{1,n}_{i-1} + \mathcal{E}^n_{i+1} + \mathcal{E}^n_{i-1}) \end{aligned}$$

So the flux stays limited if the above expression on the right hand side is always negative. This is the case, if the CFL condition $\Delta t \leq \frac{\Delta x}{c}$ is fulfilled and the following holds for all i

$$\begin{aligned} (-1 \mp 1)\mathcal{F}^{1,n}_i + (1 \pm \chi^n_i)\mathcal{E}^n_i \geq 0, \\ (1 \mp 1)\mathcal{F}^{1,n}_i + (1 \mp \chi^n_i)\mathcal{E}^n_i \geq 0, \end{aligned}$$

All of them are fulfilled. First of all we have $(1-\chi_i^n)\mathcal{E}_i^n \geq \frac{1}{3}\mathcal{E}_i^n \geq 0$, under condition (2.26). Second, we see that the expression $\pm 2\mathcal{F}_i^{1,n} + (1+\chi_i^n)\mathcal{E}_i^n$ is always positive under condition (2.26), by looking at the function (divide by $\mathcal{E}_i^n > 0$. For $\mathcal{E}_i^n = 0 \Rightarrow \mathcal{F}_i^n = 0$ and the above inequalities hold trivially)

$$h^{\pm}(z) = \pm 2z + 1 + \frac{3+4z^2}{5+2\sqrt{4-3z^2}}, \quad -1 \leq z \leq 1$$

In the interval $[-1,1]$ the function $h^{\pm}$ is continuous and therefore has a minimum. The derivative of this function is nonzero for all $z \in (-1,1)$. Furthermore, we have that $h^{\pm}(\mp 1) = 0$ and $h^{\pm}(\pm 1) = 4$. From this we conclude that $h^{\pm}(z) \geq 0$ for $|z| \leq 1$. Summarizing, we have shown that $\pm\mathcal{F}_i^{1,n+1} - \mathcal{E}_i^{n+1} \leq 0$ and therefore that the flux stays bounded.

The explicit scheme preserves the steady states up to machine precision. First of all, the radiation fluxes are all equal to zero at the steady state. Second, the radiation sources are equal to zero and stable points of the remaining ordinary differential equations. In combination with the fact that the MHD part is well-balanced (see [3]) we have that steady states are preserved up to machine precision.

The proof of flux limitation and steady state preservation for the implicit scheme is very similar to the above proof for the explicit scheme and we omit it here.

□

The numerical experiments for (1.6) fall into two different categories. First we test and compare the explicit and semi-implicit scheme described above for wave propagation. It turns out that the semi-implicit solver is several orders of magnitude more efficient in comparison with the explicit solver for radiation hydrodynamics/MHD. The second category consists of a suit of numerical experiments showing the effects of radiation on wave propagation in stratified magneto-atmospheres.

3. **Numerical experiments in 1 dimension/Efficiency study.**

In this section we present numerical experiments for testing how robustly and efficiently our schemes of type (2.1) work, comparing the explicit $M_{\mathrm{HLLC}}R_{\mathrm{HLL}_e}$ with the semi-implicit $M_{\mathrm{HLLC}}R_{\mathrm{HLL}_i}$ solver. We show that for the radiation hydrodynamic/MHD equations (1.6) the semi-implicit solver is several orders of magnitude more efficient than the explicit solver.

To begin with, we compare our numerical schemes for radiation hydrodynamics, given by (1.6) with a zero magnetic field $\tilde{\mathbf{B}} = \mathbf{0}$. The initial conditions are a discrete version of the steady state background (1.10) with $\gamma = 5/3, a = 1, p_0 = 1.13, H = 0.158$ and a gravity constant of $g = 2.74$. Furthermore, we choose $\sigma(z,t) = \frac{\rho(z,t)}{\rho(0,0)}$, so that the medium is opaque at the bottom $z = 0$ at time $t = 0$. The domain is given by $z \in [0,1]$.

For numerical simulations concerned with wave propagation in stratified atmospheres it is desirable, if not necessary, to use a well-balanced finite volume scheme, see [3]. As shown in theorem 2.1, both the explicit $M_{\mathrm{HLLC}}R_{\mathrm{HLL}_e}$ and the semi-implicit $M_{\mathrm{HLLC}}R_{\mathrm{HLL}_i}$ preserve the steady state discretely, and are therefore suitable for our task. On top of this steady state background we model the waves by introducing a local sinusoidal (in time) driving of the velocity field perpendicular to the boundary, given by the following boundary condition for the normal velocity at the bottom

$$u_3(0,t) = 0.3\sin(6\pi t). \tag{3.1}$$

As time evolves, those waves move up through the domain and are modified by the stratified RMHD equations. In figure 2 we present the results for the well-balanced explicit $M_{\mathrm{HLLC}}R_{\mathrm{HLL}_e}$ and semi-implicit $M_{\mathrm{HLLC}}R_{\mathrm{HLL}_i}$ schemes at time $t = 0.8$ for different meshes. We can see that the waves are resolved very well and the semi-

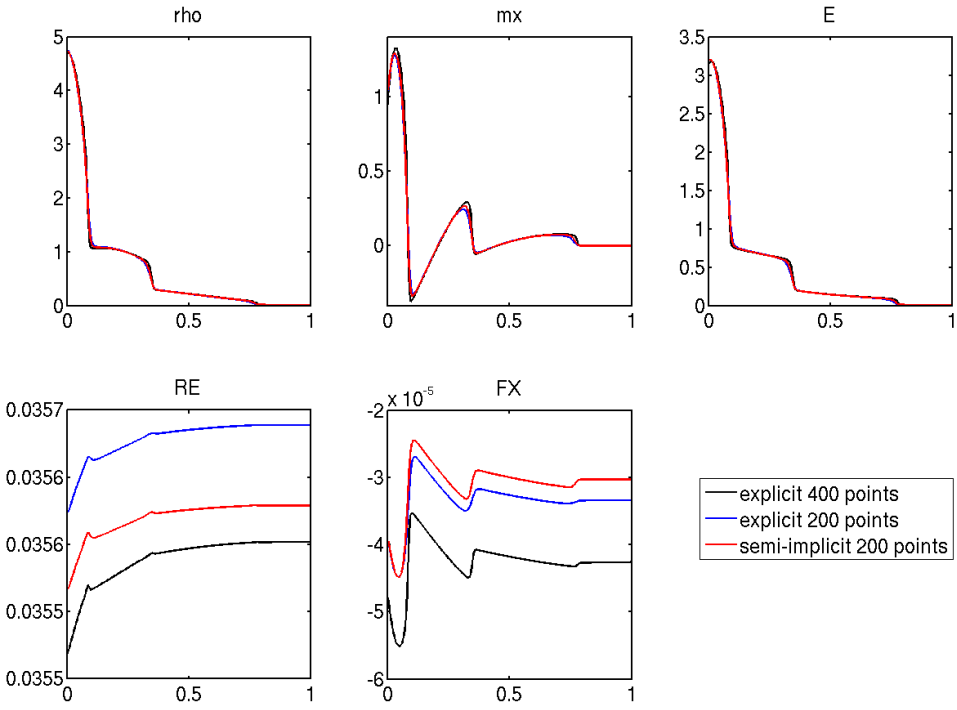

FIGURE 2. Comparison of explicit solver $M_{\mathrm{HLLC}}R_{\mathrm{HLL}_e}$ with semi-implicit solver $M_{\mathrm{HLLC}}R_{\mathrm{HLL}_i}$ for different CFL numbers at time $t = 0.8$. From top to bottom and left to right: density ρ, momentum m_3, energy E, radiative energy $\mathcal{E}$ and radiative flux $\boldsymbol{\mathcal{F}}$.

implicit solver seems to have slightly more accuracy compared to the explicit solver on the same grid, at least in the plasma variables ρ, m_3 and E, despite the fact that it uses much less computational time.

To quantify the efficiency of the explicit $M_{\mathrm{HLLC}}R_{\mathrm{HLL}_e}$ compared with the semi-implicit $M_{\mathrm{HLLC}}R_{\mathrm{HLL}_i}$ scheme, we first compute a reference solution with the explicit scheme on a very fine grid. Then we plot the computational time over the relative errors with respect to this reference solution for both the explicit and semi-implicit scheme on different mesh resolutions. We can learn from figure 3 that for the same relative error the explicit $M_{\mathrm{HLLC}}R_{\mathrm{HLL}_e}$ solver is $\mathcal{O}(10^4)$ slower compared with the semi-implicit $M_{\mathrm{HLLC}}R_{\mathrm{HLL}_i}$ solver. The reason for this tremendous difference in efficiency is the following. The maximum eigenvalue of the hydrodynamic equations compared to the speed of light is $c/\max(\lambda_{\mathrm{hydro}}(t)) = \mathcal{O}(10^4)$. That means we do $\mathcal{O}(10^4)$ more time steps with the explicit solver. There is no loss of accuracy due to the large time steps because the waves in stratified RMHD (1.6) are induced by a forcing of the hydrodynamic variable u_3. Therefore, the waves in the radiation variables $\mathbf{U}^{rad}$ are rather weak and without strong shocks, and the radiation part

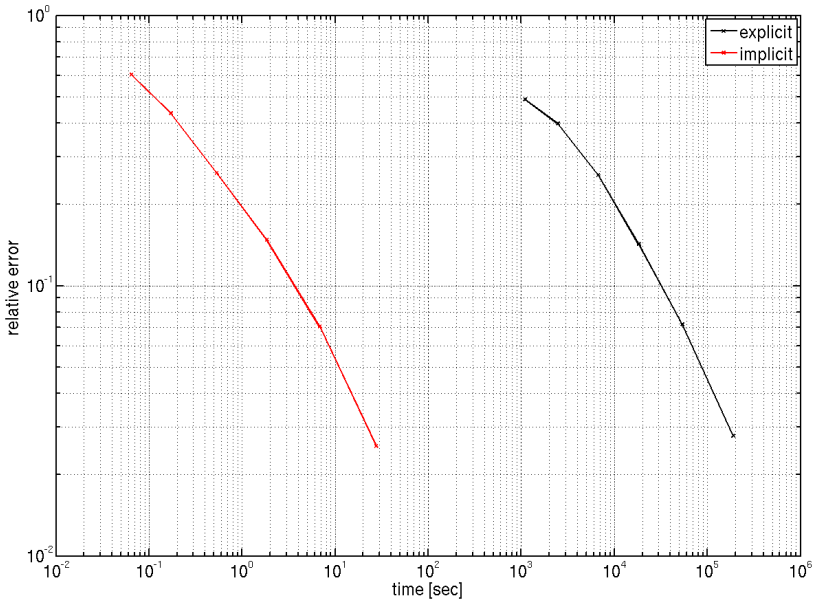

FIGURE 3. Comparison of the efficiency of the explicit $M_{\mathrm{HLLC}}R_{\mathrm{HLL}_e}$ and semi-implicit $M_{\mathrm{HLLC}}R_{\mathrm{HLL}_i}$ solver for the solution at time $t = 0.8$. The relative error is the sum of the relative errors of all variables (divided by number of variables).

can be well approximated by a rather diffusive implicit solver. We can conclude that the higher cost of solving a system of nonlinear equations at each time step is more than compensated for by allowing much larger time steps. So in this case the semi-implicit scheme $M_{\mathrm{HLLC}}R_{\mathrm{HLL}_i}$ clearly wins over the explicit version in terms of efficiency.

In the next section we focus on the influence of radiative transfer on wave propagation in stratified atmospheres.

4. **Numerical experiments in 2 dimensions/Comparison of MHD with radiation MHD.** In this section we compare the solution of the MHD equations with the solution of the RMHD equations on a suit of numerical experiments using the explicit solver $M_{\mathrm{HLLC}}R_{\mathrm{HLL}_e}$. The first order scheme is run with a CFL number of 0.45 and for the constants in the model we choose for the acceleration due to gravity, $g = 2.74$, constant $H = 0.158$, gas constant $\gamma = 5/3$ and initial pressure $p_0 = 1.13$. All subsequent two-dimensional experiments are performed on the domain $[x, z] \in [0, 4] \times [0, 1]$. Again, we choose $\sigma(z, t) = \frac{\rho(z,t)}{\rho(0,0)}$, so that the medium is opaque at the bottom $z = 0$ at time $t = 0$.

We want to compare the MHD equations with the radiation MHD equations (1.6). Since we are concerned with wave propagation in startified atmospheres we follow the setup described in articles [1, 2, 3]. We choose a discrete version of the steady state (1.10) with different background magnetic fields $\tilde{\mathbf{B}}$. A small part of the bottom boundary acts a piston and sends in temporally sinusoidal waves,

perturbing the steady state. Those boundary conditions are given by a forcing in the normal velocity field, namely

$$u^3(x,0) = 0.3e^{-100(x-1.9)^2} \sin(6\pi t)\, \mathbf{1}_{\{[1.65,2.15]\}}. \tag{4.1}$$

We start with the simplest case, i.e. in absence of a magnetic field.

4.1. **Hydrodynamics vs radiation hydrodynamics.** The setup in the pure hydrodynamic case is given by chosing the embedded magnetic field $\tilde{\mathbf{B}}$ to be zero. The results are shown in figure 4. The top row depicts the solution at time $t = 1$ for standard hydrodynamics and the bottom row the one for hydrodynamics combined with the M1 model. In order to better compare the two cases, the solution for each variable uses the same scaling for MHD and RMHD in the figure. By comparing

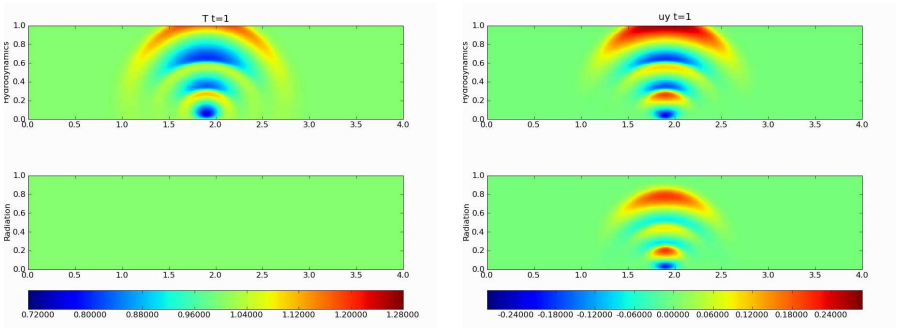

FIGURE 4. Comprison of hydrodynamics with radiation hydrodynamics. Solution from the explicit solver $R_{\mathrm{HLL}_e S_i}$ at $t = 1$ for 400×100 mesh points. Left: relative temperature change. Right: vertical velocity u_3. Each variable has the same scaling for MHD and RMHD.

the plots for temperature in figure 4 we can immediatly see that the temperature variations introduced by the boundary conditions (4.1) of radiation hydrodynamics are too small to be seen compared to the results of hydrodynamics. This means that radiative transfer compensates the (by the boundary conditions) introduced temperature variations. This has a profound effect on the velocity of the wave fronts propagating through the medium. We can see on the right of figure 4 that the first wave front for hydrodynamics without radiation is about to exit the domain on the top at time $t = 1$. In contrast, the velocity plot for radiation hydrodynamics at the same time $t = 1$ reveals that the leading wave front is still a distance away from the top boundary and is therefor clearly propagating with a slower speeed due to the action of radiative transfer. Furthermore, we can see that the amplitude of the velocity disturbances is reduced if we account for radiative transport. The overall dynamics are, however, comparable for both cases.

We continue by studying the effects of radiative transport in the case of complicated nontrivial magnetic fields.

4.2. **Comparison of MHD with Radiation MHD.** The above experiment was the comparison of hydrodyamics with radiation hydrodynamics since the magnetic field stayed zero during the whole computation. In order to see the effect of radiative

transfer on the solution of the MHD equations in two dimensions, we choose a *realistic* two-dimensional background magnetic field in the following way. We let $\widetilde{B}_3(x,0,0)$ approximate

$$\widetilde{B}_3(x,0,0) = 2.7e^{-7.2r^2} - 1.3e^{-40(r-0.6)^2},\ r = |x-2|, x \in [0,4] \tag{4.2}$$

by using a Fourier expansion of vector harmonic functions (see also [1, 2, 3]), i.e.

$$\widetilde{B}_1(x,y,z) = \sum_{l=0}^{L} f_l \sin(2\pi l x)\, e^{-2\pi l z}, \quad \widetilde{B}_3(x,y,z) = \sum_{l=0}^{L} f_l \cos(2\pi l x)\, e^{-2\pi l z}, \quad B_2(x,y,z) \equiv 0, \tag{4.3}$$

where the f_l's are Fourier coefficients corresponding to the background magnetic field at the bottom of the domain and L is the total number of Fourier modes.

The computations presented here use the first fourteen terms in the Fourier series. The full magnetic field $\widetilde{\mathbf{B}}(x,y,z)$ follows then from the potential field assumption, i.e. (4.3). The resulting potential field consists of a large unipolar magnetic flux concentration surrounded on each side by two smaller concentrations of opposite polarity field (see[1], figure 1 for an illustration). The rest of the constants and σ is chosen as in the case above.

The numerical results are presented in figure 4.2. Again, each variable is scaled in the same way, in order to allow for a good comparison of the solutions of MHD and RMHD. As is expected (see [1, 2, 3]), the waves are more focused compared to

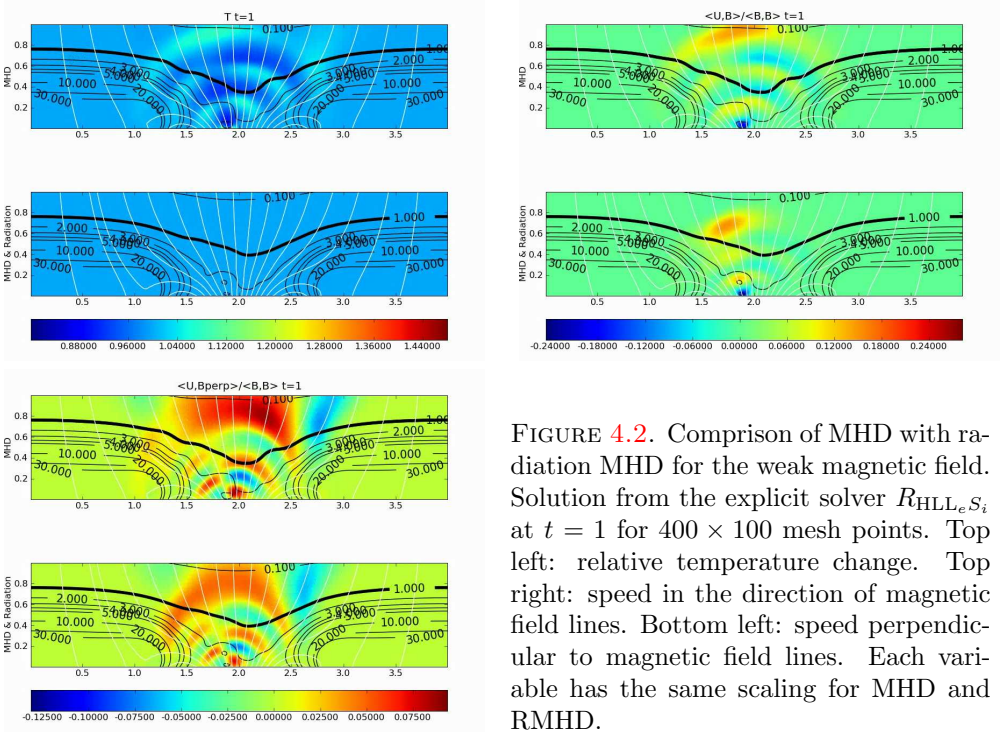

FIGURE 4.2. Comprison of MHD with radiation MHD for the weak magnetic field. Solution from the explicit solver $R_{\mathrm{HLL}_e S_i}$ at $t = 1$ for 400×100 mesh points. Top left: relative temperature change. Top right: speed in the direction of magnetic field lines. Bottom left: speed perpendicular to magnetic field lines. Each variable has the same scaling for MHD and RMHD.

the hydrodynamics case due to the presence of the nonzero magentic field. Looking at the temperature plot, we again see that the radiative transport results in an almost constant temperature distribution compared to the solution of the standard MHD equations. Looking at the velocity in the direction of the magentic field, we again see that the wave fronts are propagating with a smaller speed in the case of RMHD. This difference is less prominent if we consider the velocity perpendicular to the magentic field.

In this example the magentic field is still of moderate strength. We therefor increase our the magnetic field (4.2) by a factor of 3. The results are presented in figure 4.2. In this case the waves are even more focused due to the action of the Lorentz force, and follow the magnetic field lines (white). As before, it becomes

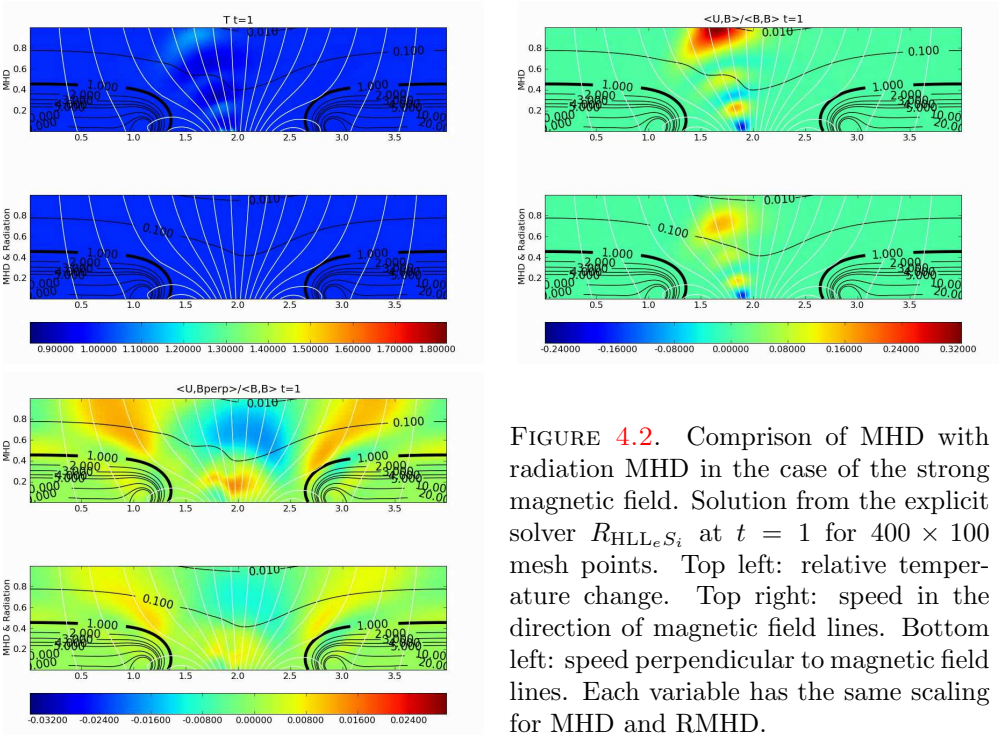

FIGURE 4.2. Comprison of MHD with radiation MHD in the case of the strong magnetic field. Solution from the explicit solver $R_{\mathrm{HLL}_e S_i}$ at $t = 1$ for 400×100 mesh points. Top left: relative temperature change. Top right: speed in the direction of magnetic field lines. Bottom left: speed perpendicular to magnetic field lines. Each variable has the same scaling for MHD and RMHD.

apparent from the temperature plot that the temperature is kept almost constant in the case of RMHD in contrast to the solution of the MHD equations. Looking at the velocity in the direction of the magnetic field, we can again conclude that the overall behaviour is the same, but the speed of the wave fronts as well as the amplitude of them is reduced due to radiative transfer. This can also be seen in the plot for the velocity in the direction perpendicular to the magnetic field.

5. **Conclusion.** Wave propagation in the solar atmosphere is a very important mode of energy transport in the sun and plays an essential role in many interesting solar phenomena, particularly in chromospheric and coronal heating. Solar wave

propagation can be modeled in terms of the equations of stratified radiative MHD. As the standard radiative transport equation is high-dimensional, reduced models are preferred. We focus on a particular reduced model, the so-called M1 model that accounts for radiation in terms of spectral radiative moments. The resulting M1-stratified MHD coupled system is then simulated using numerical schemes.

We consider two sets of numerical schemes in this paper. Both schemes are based on the coupling between the MHD and radiation parts in terms of source terms. Thus, standard HLLC and two-wave HLL solvers can be used to form the numerical fluxes in a finite volume framework. The simplest form of time stepping is the forward Euler time stepping. It has to augmented with implicit treatment of the stiff radiative source term. The resulting scheme works quite well. However, it is computationally very expensive as the relevant speed of the system, that is used in setting the time step through the CFL condition for the explicit scheme, is given by the speed of light. This is three to four orders of magnitude larger than the fastest magneto sonic waves of the system.

Consequently, we couple an explicit forward Euler discretization of the MHD flux and source terms with an implicit backward Euler discretization of the radiative flux and source terms. This coupled semi-implicit scheme allows us to determine the time step in terms of the magneto sonic waves and allows for time steps that are orders of magnitude larger than the fully explicit scheme. Numerical experiments show that the semi-implicit scheme is three to four orders of magnitude more efficient than the fully explicit scheme.

We conclude with a suit of numerical experiments for the propagation of waves in the sun. Both weak and strong magnetic fields are used and the numerical experiments indicate that the schemes work quite well with sharp resolution of the waves. Compared to the absence of radiation, adding radiation implies greater uniformity in temperature distributions as a consequence of radiative cooling. Furthermore, this cooling leads to the slowing down of propagating waves. Furthermore, the wave amplitude is also reduced as energy is taken out of the system on account of radiative cooling. This energy loss poses a considerable obstacle for wave propagation explaining coronal heating. More elaborate physical mechanisms are needed to explain this heating.

In terms of implementation, we use a Newton method to solve the resulting nonlinear algebraic system of equations at each time step. Currently, a direct method for inverting the linearized equations within each Newton step, is used. However, practical efficiency dictates the use of an iterative krylov type methods for solving the resulting linear equations. Such iterative methods suffer from ill-conditioning. The design of an efficient preconditioner is a prerequisite for the efficient solution of the nonlinear equations and will be the subject of a forthcoming paper.

REFERENCES

[1] T. J. Bogdan *et al.* Waves in the magnetized solar atmosphere II: Waves from localized sources in magnetic flux concentrations. *Astrophys. Jl,* 599, 2003, 626 - 660.

[2] F. Fuchs, A. D. McMurry, S. Mishra, N. H. Risebro and K. Waagan. Finite volume schemes for wave propagation in stratified magneto-atmospheres. *Comm. Comput. Phys.,* 7 (3), 2010, 473-509.

[3] F. Fuchs, A. D. McMurry, S. Mishra, N. H. Risebro and K. Waagan Well-balanced high-order finite volume methods for simulating wave propagation in stratified magneto-atmospheres. *Jl. Comput. Phys.,* 229 (11), 2010, 4033-4058.

[4] D. Mihalas and G. Mihalas. Foundation of Radiation Hydrodynamics. *Oxford university press,* Oxford, 1984.

[5] B. Dubroca and J. L. Feugeas. Entropic moment closure hierarchy for the radiative transfer equations. *C. R. Acad. Sci Paris*, Ser 1, 329, 915-920, 1999.
[6] C. Berthon, P. Charrier and B. Dubroca. An HLLC scheme to solve the M1 model of radiative transfer in two space dimensions. *Jl. Sci. Comp.,* 31 (3), 347-389, 2007.

Recent Research Reports

Nr.	Authors/Title

2013-30 R. Hiptmair and A. Paganini and S. Sargheini
Comparison of Approximate Shape Gradients

2013-31 R. Hiptmair and A. Moiola and I. Perugia
Plane Wave Discontinuous Galerkin Methods: Exponential Convergence of the hp-version

2013-32 U. Koley and N. Risebro and Ch. Schwab and F. Weber
Multilevel Monte Carlo for random degenerate scalar convection diffusion equation

2013-33 A. Barth and Ch. Schwab and J. Sukys
Multilevel Monte Carlo approximations of statistical solutions to the Navier-Stokes equation

2013-34 M. Hutzenthaler and A. Jentzen and X. Wang
Exponential integrability properties of numerical approximation processes for nonlinear stochastic differential equations

2013-35 S. Cox and M. Hutzenthaler and A. Jentzen
Local Lipschitz continuity in the initial value and strong completeness for nonlinear stochastic differential equations

2013-36 S. Becker and A. Jentzen and P. Kloeden
An exponential Wagner-Platen type scheme for SPDEs

2013-37 D. Bloemker and A. Jentzen
Galerkin approximations for the stochastic Burgers equation

2013-38 W. E and A. Jentzen and H. Shen
Renormalized powers of Ornstein-Uhlenbeck processes and well-posedness of stochastic Ginzburg-Landau equations

2013-39 D. Schoetzau and Ch. Schwab and T.P. Wihler
hp-dGFEM for Second-Order Mixed Elliptic Problems in Polyhedra